



## Fast Phosphate Adsorption on Pectin-Ammonium Functionalized Mesoporous Silica Hybrid Material

Sh. El Raffie<sup>a</sup>, Hosni Ibrahim<sup>b</sup>, Marwa S. Shalaby<sup>a</sup>, Ola Roshdy<sup>b</sup> and Marwa H. Gaber<sup>a\*</sup>

<sup>a</sup> Chemical Engineering and Pilot Plant Department, National Research Centre - ElBuhouth St., Dokki, Giza, Egypt

<sup>b</sup> Chemistry Department, Faculty of Science, Cairo University, Egypt



CrossMark

### Abstract

Mesoporous silica nanoparticles are one of the most promising adsorbents for metal ions due to their ultrahigh surface area, outsized pore size, and miscellaneous composition. However, their applications remain limited as a frail ion exchanger for anion adsorption due to the existence of silanol groups on the surface in order to overcome these drawbacks, hybrid organic-inorganic silica material with high specific surface area, highly adsorptive capacity, and good chemical and thermal stability was prepared. We report here a facile method for the preparation of newly amine functionalized silica-pectin hybrid material. To better understand about the surface modification of the silica gels, the analysis of materials' surfaces was conducted using Fourier Transform Infrared Spectroscopy (FTIR), X-ray diffraction (XRD), Scanning Electron Microscopy (SEM), transmission electron microscopy (TEM). The results showed that  $\text{PO}_4^{3-}$  adsorption increased with reaction time and temperature while it decreased with an increase in solution pH. Adsorption isotherm data exhibited good agreement with the Freundlich model with maximum monolayer adsorption capacities of  $98.9 \text{ mg l}^{-1}$  (P-AFSF).

**Keywords:** phosphate, pectin, functionalized silica, adsorption, wastewater.

### 1. Introduction

Mesoporous silica has been well developed and attracted a vast deal of interest in a diversity of important applications, since it was founded by Mobil scientists and Kuroda and his co-workers [1], owing, for example, to large pore diameters tunable in size from 2 to 50 nm, highly specific surface areas, and compositions [2]. Well-ordered mesostructured silica is generally promoted by the formation of surfactant aggregates (micelle) templating mechanism, in which the surfactants serve as a structure-directing agent (SDA). Electrostatic charge-matching and electrically neutral pathways are proposed for the templating mechanism [3, 4]. Mesoporous silica materials are obtained after the (SDA) removal by extraction or calcinations from the mesostructured silica-micelle composite. It has several advantages to be an ideal adsorption such as highly ordered structures, structure versatility, and high surface area, tunable pore size [5], however, their applications for

adsorption remains limited, because of its low adsorptive capacity of the surface groups Si-OH binding phosphate anions [6]. Several preceding approaches projected to increase the adsorption capacity have been made to improve their capacity, for example, synthesis of Fe (III)-coordinated ethylenediamine-functionalized mesoporous silica improved the adsorption efficiency of phosphate adsorption as P [7]. Adsorption can therefore be improved by synthesis of iron functionalized silica loading various diamino groups to improve the binding affinity with p ion [8], but this approach comes with a number of drawbacks such as decreased pore size, limited diffusion, and monotonous process[9]. Recently, the variety of organic macromolecules such as polystyrene and P123 have been used to generate mesopores and macropores in the adsorbents. The macropores material act as fast carrier conduits to the surface of mesopores thus enhances the mass transport and increase the

\*Corresponding author e-mail: [chem\\_mero\\_hosni@yahoo.com](mailto:chem_mero_hosni@yahoo.com)

Receive Date: 24 September 2020, Revise Date: 21 October 2020, Accept Date: 01 November 2020

DOI: 10.21608/EJCHEM.2020.43996.2892

©2021 National Information and Documentation Center (NIDOC)

diffusion rate [10]. However, the composites synthesized by this method have not nanosized pores, and involves complex attachment of hazardous reagents [11]. Beside organic macromolecules, biomaterials (for example, polysaccharides, chitosan, and protein) have been used for biomimetic functionalization for mesoporous materials for the removal of heavy metals [12]. However, it has been a great challenge to remove tetrahedral toxic oxyanion because the anions with a similar structure, such as nitrate, sulfate and phosphate, often coexist in environment with high concentrations [13]. As understood from earlier works in the literature, there are several adsorption studies based on amino functionalized silica composites, but to the best of our knowledge, the usage of pectin –amino functionalized silica composites for phosphate anion removal has not been liberated in the past in this regard as well. Hence an attempt has been made to analyze and compare the efficiency of functionalized silica gels, modified with aminopropylethoxysilanes and pectin in the process of phosphate removal. The studies have been performed in artificial wastewater conditions to understand the trend of phosphate anions removal with respect to the effect of temperature, time, concentration and adsorption dose as well. The excessive amounts of phosphorus (P) in water bodies cause the problem of algae growth (eutrophication) [14]. The water quality is affected and decreased due to this phenomenon which in turn increases the cost of water treatment [15]. The load of P discharged to water bodies comes from agricultural activities and use of fertilizers, domestic and industrial wastewater, and atmospheric deposition [16]. Reduction of runoff from agricultural usage of land and atmospheric deposition are complex problems better solved by economical and technical means rather than technically [17]. We hypothesize that the pectin- amino functionalized mesoporous silica (P-AFS) composite is one of the most effective and selective methods for phosphate anion accumulation.

## MATERIALS AND METHODS

### Chemicals

Commercial pectin (100g, from, loba, chemie, india.), 3-Aminopropyl triethoxysilane  $\text{H}_2\text{N}(\text{CH}_2)_3\text{Si}(\text{OCH}_3)_3$  (APTES 97% from Aldrich), tetraethyl orthosilicate (TEOS 99% from Aldrich) CTABr (hexadecyltrimethylammoniumbromide, Sigma-

Aldrich) as a structure-directing agent and were used for the functionalization of silica gel. The other chemicals incorporated analytical grade Toluene, Methanol, and Ethanol (purity for all, >99.5%) are provided from El-Nasr Pharmaceutical Company, Egypt. The synthetic wastewater used for the adsorption studies in this paper was prepared from (calcium hydroxide, potassium phosphate monobasic ( $\text{KH}_2\text{PO}_4$ ), barium chloride dihydrate, magnesium sulphate, sodium bicarbonate, sodium chloride, aluminum chloride hexahydrate)

### Mesoporous silica MCM-48 synthesis

The complete synthesis was carried out in a 500 mL round-bottom flask set with a magnetic stirrer. In which two different solutions were prepared. First, the surfactant solution, CTABr was dissolved slowly in 100 ml of dehydrated ethanol and deionized water mixture, gently stirring used to avoid the formation of bubbles and make solution (a). Next, 100 ml of NaOH, 50 ml of deionized (DI) water, and 50 ml of dehydrated ethanol were mixed together by stirring at a speed of 200 rpm, then 50 ml of tetraethoxysilane (TEOS) was mixed with 100 ml of dehydrated ethanol. The mixture was poured quickly into the solution to form solution (b). Solution (b) was added drop-by-drop into solution (a) and stirred for 1 h; till solution becomes cloudy. A white gel was formed after few minutes and transferred to a Teflon container. The product was placed in a sealed metal autoclave vessel subjected to hydrothermal synthesis at 373 K in a preheated oven for 4 days. The solid yield was then filtered, washed with hot water, and dried overnight. For the removal of the surfactant, the final product was calcined at 813 K with a heating rate of 1 K/min in air for 6 h [18].

### Amine functionalization

For dry grafting, 6 g of MCM-48 powder was dispersed in 100 mL of dry toluene in a 500 mL twin-neck round-bottom flask under continuous stirring (400 rpm) in an Argon atmosphere during 15 min. according to the method in previous literatures [18, 19], then the flask was immersed in a temperature controlled oil bath. When the mixture reached to 383 K, 5 ml amine silane agent was added and stirred for 1 h under reflux. The solid product was vacuumed, filtered, washed with dichloromethane/ diethyl ether (1:1) mixture and dried at 323 K for 12 h.

### Synthesis of pectin- amine functionalized silica complex

The method for synthesis of P-AFS was modified according to Katavet al. The first step performed was to reduce the degree of esterification, DE, of the raw PT through an alkaline hydrolysis reaction. An accurately amount of PT was solubilized in NaOH aqueous solution (molar ratio PT/NaOH equal 1:1). The hydrolysis reaction was kept under magnetic

stirring, at 50 °C for 24 h. After this, the PT was collected through precipitation in ethanol and then dried by lyophilization process (Christ Gefriertrocknungsanlagen equipment, at -55 °C for 24 h). From the PT deesterified it was prepared an aqueous solution (2wt %) in which were added 6 mL of ED (molar ratio between carboxyl groups on PT/ED 1:50). The resultant solution was stirred vigorously until the complete homogenization. Homogeneous mixture of an accurately amount of amine functionalized silica (10g) have been dispersed in 100 mL of dry diethyl ether under ultrasonication for 10 to 35 min and the deesterified pectin was stirred under reflux for 24 h. After being filtered, the solid product was soxhlet extracted with methanol, and dichloromethane for 6 h, respectively. The product was then dried under vacuum at 70°C over 12h.

#### **Powder x-ray diffraction**

PXRD patterns of the prepared samples were recorded using a Bruker-D8 Advanced diffractometer with Cu-K $\alpha$  radiation ( $\lambda = 1.78897 \text{ \AA}$ ). The samples were scanned in the  $2\theta$  range of 5° to 80° using a step size of 0.02° and a scan speed of 0.4 s per step in a continuous scanning mode.

**Scanning electron microscopy:** SEM micrographs of the samples were acquired using a JEOL JSM-6010LA InTouchScope microscope. The pieces surfaces were coated with gold by sputtering, to make them electrically conductive and allow viewing by SEM.

**Transmission electron microscopy:** TEM micrographs of the materials, after surfactant extraction, were recorded with a JEOL 2000FX transmission electron microscope. The TEM samples were prepared by grinding the sample and mixing with a small amount of absolute ethanol. The solution was allowed to settle and lacey carbon TEM grids (Ted Pella Inc) were used to scoop some of the clear liquid and then allowed to dry. This was done so that the smallest particles could be mounted on the grid for better TEM analysis. The energy dispersive X-ray spectroscopy (EDX) data obtained with the integrated scanning TEM (STEM) unit and attached EDAX spectrometer.

**Fourier transform infrared (FTIR) spectroscopy** of the fresh samples (not dehydrated) were performed with a Bruker Vertex 70 FTIR spectrometer equipped with a deuterated triglycine sulfate (DTGS) detector and a Golden Gate diamond attenuated total reflectance (ATR) accessory. Spectra were recorded by averaging 100 scans in the 4000–600  $\text{cm}^{-1}$ .

#### **Gas adsorption isotherms**

All nitrogen sorption measurements in this work were performed with an ASAP 2010 instrument

(Micromeritics), at 77 K. Autosorb 1 software (Quantachrome instruments) was used to determine surface area by BET theory, and NLDFT theory was the basis for pore size and the pore size distribution location.

#### **Batch adsorption studies**

Adsorption equilibrium was achieved after adding a certain amount of the samples PT, AFS and P-AFS to 0.2 L of phosphate synthetic solution with a given initial concentration ( $C_0$ ). The resulting mixture was placed in a temperature-controllable magnetic stirrer at 400 rpm to begin the adsorption. The adsorption experiments were performed for 30 min to ensure that the adsorption reached the equilibrium. After sorption, all samples were filtered through ashless filter paper prior to analysis. The supernatant was acidified with 0.5 M  $\text{HNO}_3$  and stored in acid washed bottles. The residual  $\text{PO}_4^{3-}$  concentration in solution was measured using the ascorbic acid method [19] using UV spectrophotometer (agilent Cary 100 UV-vis) at a wavelength of 880 nm. The adsorption capacity at equilibrium was denoted as  $q_e$  ( $\text{mg}\cdot\text{g}^{-1}$ ) and calculated using the following equations:

$$q_e = \frac{C_0 - C_e}{M} V \quad (1)$$

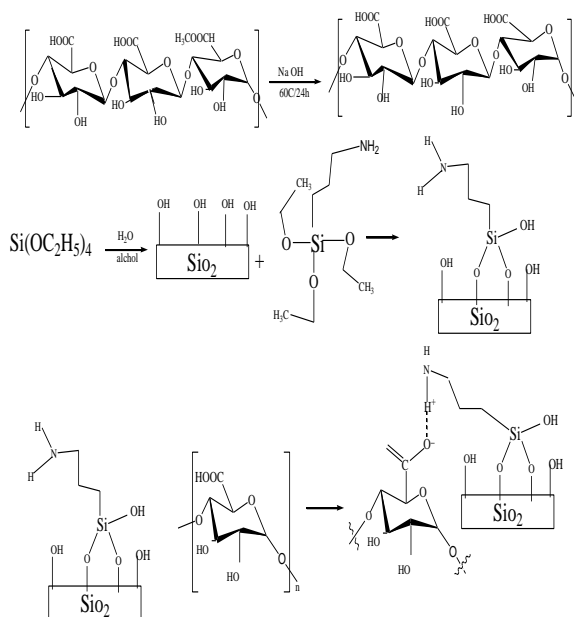
$$\% \text{ Removal} = \frac{C_0 - C_e}{C_0} \times 100 \quad (2)$$

Where  $C_0$  and  $C_e$  represent the initial and residual  $\text{PO}_4^{3-}$  ion concentration ( $\text{mg}\cdot\text{l}^{-1}$ ) in the liquid phase,  $V$  is the volume of the solution (L), and ( $M$ ) is the mass of the composite adsorbent.

### **Results and Discussions**

#### **Synthesis and characterizations of P-AFS**

Briefly, the (P-AFS) was prepared via a hard-template method. The composite material was obtained in two steps. The amino-functionalized mesoporous silica (AFS) was produced via a grafting step. Two monomers of 3-aminopropyl triethoxysilane APTES and TEOS were prearranged under the control of CTABr (Materials and methods). The cloudy formed gel with a quantity of 100 g was subjected to hydrothermal synthesis in a Teflon-lined stainless steel autoclaves heated at 110°C. Then the solid product was filtered, washed with hot water, and dried overnight, then calcined, to eliminate the surfactant, the resulting monodispersed raw silica was dispersed in toluene for grafting step with 3-aminopropyl triethoxysilane [20].

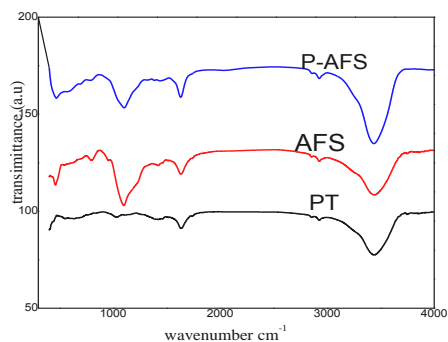


**Scheme 1. Proposed construction mechanism of (P-AFS) composite material, adopted from Yamada et al.(21)**

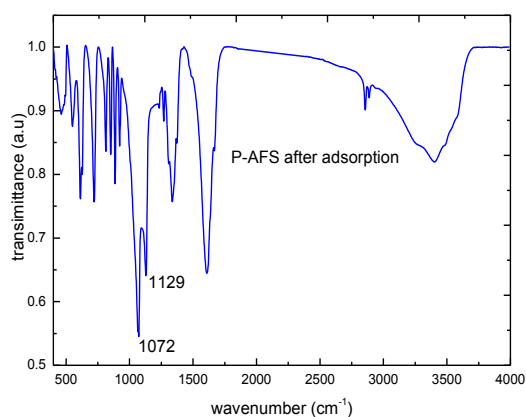
The mesoporous is synthesized with no disorders of the organosilanes yielding therefore hydrothermally more stable “compact” material. The second step involves decreasing the degree of pectin esterification via the alkaline hydrolysis reaction, then keeping the reaction mixture under magnetic stirring for 24 h for complete homogenization reaction. The construction mechanism of (P-AFS) composite material is proposed to be the  $\text{-NH}_2\text{-}$  group of the (AFS) coupled with the  $\text{-COO-}$  group of pectin by the electrostatic interaction. Additionally, the three dimensional Network structures of (AFS) encapsulate the pectin molecule in its network; as a result, the (P-AFS) composite materials provided the water-insoluble property. Scheme 1 shows the proposed structural model of (P-AFS) composite material [21].

#### Characterization of P-AFS composite

In order to get an ultimate account of the functional groups present on the surface of PT, AFS and P-AFS, the complete study of the IR plots, obtained from the surface of different samples surfaces, was performed. The graphs enlighten the spectra for PT, AFS and P-AFS are shown in Fig. (1a).



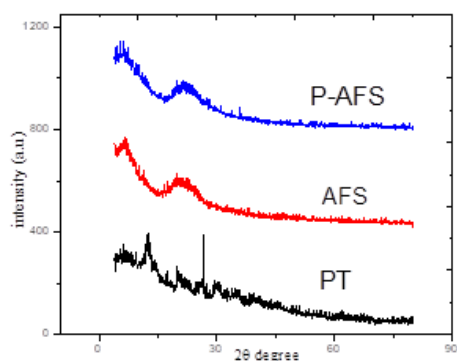
**Figure. 1a.** Fourier transform (FTIR), spectra PT, AFS, P-AFS composite a.u., arbitrary unit.



**Figure. 1b.** Fourier transform (FTIR), spectra, P-AFS composite a.u., arbitrary unit. after adsorption .

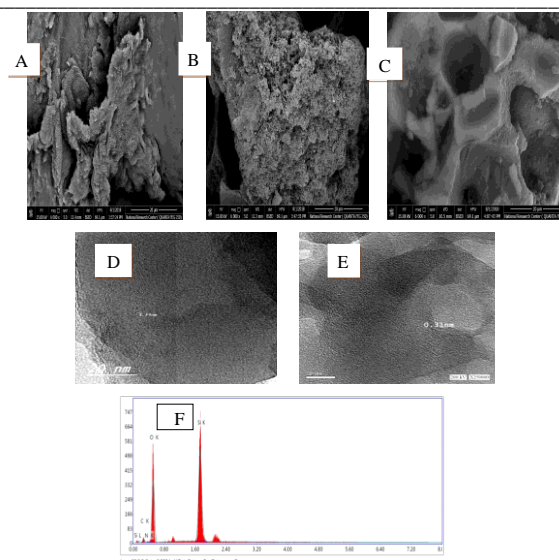
The FTIR spectrum of PT exhibited a broad band at  $3430\text{cm}^{-1}$  attributed to stretching vibration of  $\text{-OH}$  groups; a band at  $2918\text{cm}^{-1}$  attributed to stretching vibration of  $\text{C-H}$  bond ;the band at  $1751\text{cm}^{-1}$  is correlated to  $\text{C=O}$  stretching of esterified carboxylic groups ( $\text{-COOCH}_3$ ). In addition, bands at  $1411$ ,  $1101$  and  $1019\text{cm}^{-1}$  attributed to  $\text{-CH}_2$  scissoring,  $\text{-CH-OH-}$  stretching of aliphatic cyclic secondary alcohol and  $\text{-CH-O-CH-}$  stretching (Sutar et al., 2008)[26]. In AFS the grafting of the  $\text{NH}_2$  group to silica surface was confirmed by twin peaks near  $3400$  to  $3300\text{cm}^{-1}$  that are characteristic for  $\text{N-H}$  stretching, a shoulder peak appeared at  $1660\text{cm}^{-1}$  is a characteristic peak for  $\text{N-H}$  bending and the  $\text{C-H}$  bonds (at  $2931\text{-}2869\text{cm}^{-1}$ ) dependable with the functional groups used [27]. In contrast, in the (P-AFS) composite material, a new band assigned to the symmetric stretching vibration of the secondary ammonium salt at  $1643\text{cm}^{-1}$  is observed for AFS after reaction with pectin. This result indicates that  $\text{-NH-}$  group of the AFS molecule formed the  $\text{-NH}_2^+$  group by the proton from the  $\text{-COOH}$  group, and the P-AFS composite material had been produced as a result of electrostatic interaction between the  $\text{-COO}^-$  group of PT and  $\text{NH}_2^+$  group of AFS [28].

in figure(1b) Additional peaks corresponding to P = O vibration in FTIR characterization were identified at  $1072\text{ cm}^{-1}$  and  $1129\text{ cm}^{-1}$  consistent with the results in the literature.



**Figure 2.** XRD patterns of the sample PT, AFS, P-AFS composite a.u., arbitrary unit.

Fig. (2) Reveals that these samples are entirely amorphous. The (PT) present semi-crystalline patterns with more diffraction peaks were observed. The XRD patterns of AFS reveals a broad peak, suggesting that AFS is mesostructured silica with low regularity at  $2\theta=21.2^\circ$  with d spacing of 4.4 nm. According to Kim et al. in the case of mesoporous silica material, the peak intensity is a function of the scattering difference between the silica walls and the pore channels, after grafting the amino group to the pore surface of mesoporous silica, the XRD peak intensity is decreased conforming the grafting of amino group. In the P-AFS the film shows a single broad reflection at  $21^\circ$  with a d spacing of  $\sim 4.1\text{ \AA}$ . The d spacing is generally considered the packing distance between polymer chains, so the d spacing was decreased, as a result of the electrostatic interaction between cationic amino groups and anionic carboxylate head groups is increased [25,26]. Scanning electron micrographs (SEM) were acquired on PT, AFS and P-AFS in order to identify differences in their surfaces, at 300 and 12000 magnifications. As shown in Fig.(3A). PT shows a fibrous and rough morphology with a coarse aspect



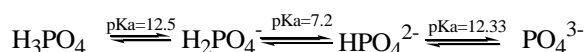
**Figure 3.** Characterization of samples. (A) SEM characterization of PT, (B) SEM characterization of AFS, (C) SEM characterization of P-AFS, (D) STEM characterization of AFS, (E and F) STEM image and EDX line scan of P-AFS.

Fig. (3B) shows the surface of AFS morphological structure, presented the formation of a large grape-like structure resultant of the polymerization process. In Fig. (3C) the structure morphology shows that the P-AFS has a porous structure with cylindrical pores with no apparent order. The formation of a nanoporous is a result of the increased solubility of the polymer in the presence of the template, which delays precipitation of the highly cross-linked gel. In Corresponding TEM images Fig. (3D) and Fig. (3E) the pores appear interconnected and wormhole-like. The particle size of AFS lies within the range of 1.5-2nm, on close observation of particle size changes after modification the P-AFS particle size lies within the range of 0.5-1 nm which represents a reduction in particle size resulting in larger surface area to improve the adsorption of anions. Energy Dispersive X-ray (EDX) was used to determine the loading of the amino group on the composite Fig. (3F). The  $\text{N}_2$  adsorption-desorption isotherm curves showed that the P-AFS follows Type IV suggesting adsorption behavior of mesoporous material along with hysteresis loops between the adsorption and desorption branch in the  $P/P_0$  range 0.3-0.9 suggesting multilayer adsorption. On the other hand, deesterified PT and AFS exhibit Type I and II curves in bare, respectively, indicating microporous materials with micropore filling with the absence of multilayer adsorption a slight hysteresis behavior in the  $P/P_0$  range 0.3-0.9 Fig. (4A). the calculated Brunauer-Emmett-Teller area of the P-AFS, PT, and AFS were  $(608.522, 207.233$  and  $405.672\text{ m}^2\text{g}^{-1}$ , respectively Fig. (4B) comprising a small amount of micropores with diameters  $(5.41, 5.1$  and  $4.2\text{ cm}^3\text{ g}^{-1}$ ,

respectively) and mainly external surface area (9.276, 3.53, and 7.048, respectively).

#### Adsorptive performance

The equilibrium batch experiments were conducted to study the efficiency of the P-AFS composite material for the adsorptive removal of  $\text{PO}_4^{3-}$  anions from wastewater with the comparative study of  $\text{PO}_4^{3-}$  anions adsorption by AFS and PT. The water-insoluble P-AFS composite material contained the hydroxyl group of PT and amino group (nitrogen atom) of AFS, which can interact with phosphate anions [27]. The adsorption experiments of  $\text{PO}_4^{3-}$  anion were conducted in order to comparatively study the activity and the situation of the amino-organic moieties introduced into AFS and P-AFS. As a control PT was tested for anion binding under similar conditions. The reusability of the P-AFS was also applicable through successive regeneration and recycle tests (Figure. 11). In addition, the effect of the solution pH on the phosphate adsorption was examined by adjusting the initial pH from 2 to 12. Fig. (5) illustrates the overall adsorption levels of PT, AFS and P-AFS. From the overall comparative study, it is shown that AFS and P-AFS modified silica yield the best possible adsorption efficiency for a given phosphate anion. The AFS showed adsorption efficiency of around 82% at the maximum pH of 8 fixed for the analysis. P-AFS recorded comparatively a little better efficiency than AFS at pH 8. This was because the variation in operating pH does not only affect the distribution of charges on the adsorbent surface but also affects the degree of ionization and dissociation of functional groups [28,29]. The pH related to the equilibrium dissociation of  $\text{PO}_4^{3-}$  in the liquid phase is given by:



It's obvious from this equation that the  $\text{PO}_4^{3-}$  species domination is dependent on the solution pH that affects the force of electrostatic attraction. Furthermore, the charges on the composite materials surfaces at a pH of point of zero charge of 3.5 for PT, 7.3 for AFS, and 8.5 for P-AFS can also explicate improved  $\text{PO}_4^{3-}$  adsorption. Wherever the positive charges mounted up under the  $\text{pH}_{\text{pzc}}$ , whilst negative charges collected over the  $\text{pH}_{\text{pzc}}$  so that burly competition occurs among  $\text{PO}_4^{3-}$  species ( $\text{H}_2\text{PO}_4^-$ ,  $\text{HPO}_4^{2-}$ , and  $\text{PO}_4^{3-}$ ) and ( $\text{OH}^-$ ) ions at elevated pH, creating physically powerful repulsions between  $\text{PO}_4^{3-}$  and hydroxyl ions so as adsorption decreased. On the other hand,  $\text{PO}_4^{3-}$  adsorption may also be motivated and improved by the existence of free ( $\text{OH}^-$ ) ions, which could be replaced by  $\text{PO}_4^{3-}$  anions on surface [30].

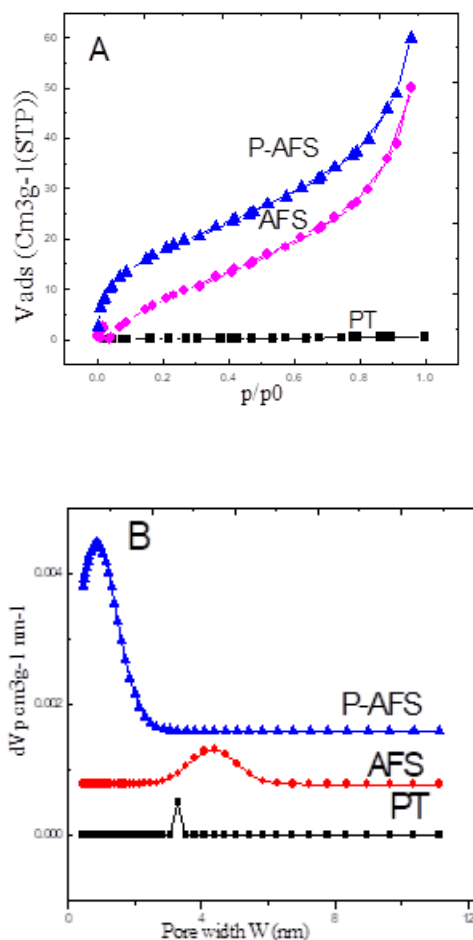
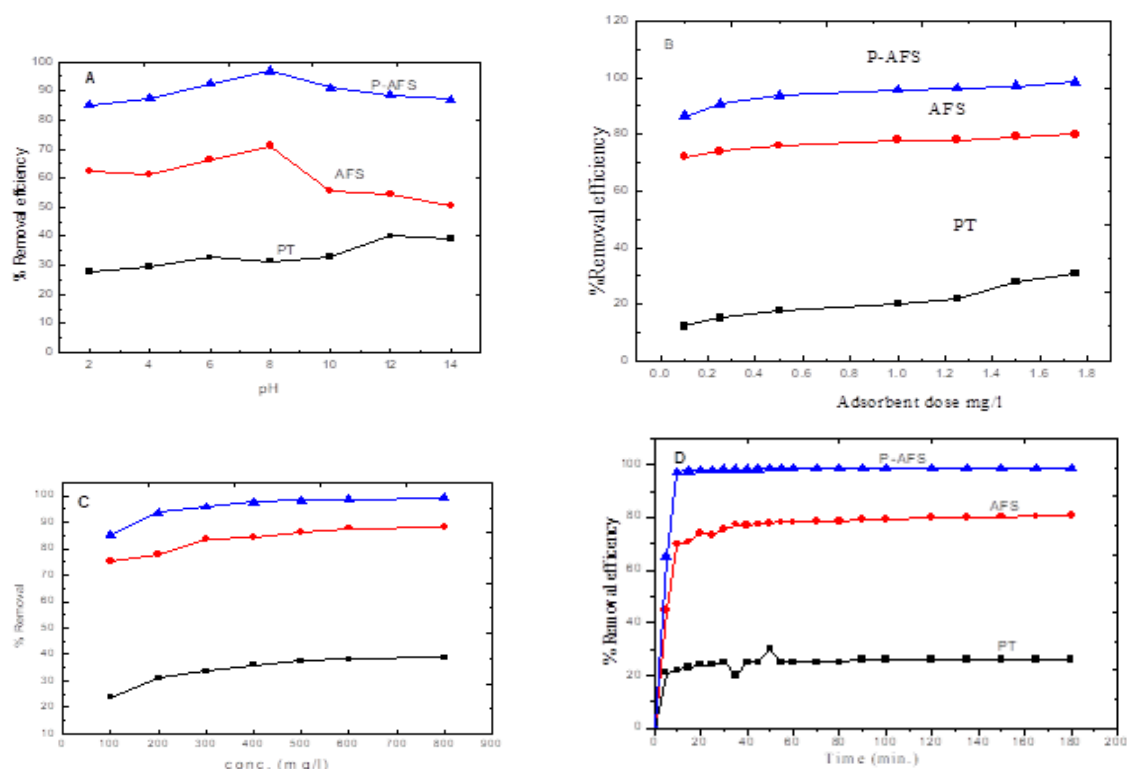


Figure. 4 (A).  $\text{N}_2$  adsorption and desorption isotherms of adsorbents at 77 and 298 K, and 4 (B) adsorbents pore diameter

#### Effect of adsorbent dose and initial concentration

The synopsis of all experiments outlined the effect of different adsorbent dosage on  $\text{PO}_4^{3-}$  adsorption from 0.1 to 1.8  $\text{mg L}^{-1}$  with an initial  $\text{PO}_4^{3-}$  concentration of 27.72  $\text{mg L}^{-1}$  at  $\text{pH } 7.0 \pm 1.0$  and 25  $^\circ\text{C}$  are sketched in Fig. (5). It is obvious that the increase in  $\text{PO}_4^{3-}$  removal is achieved by the increase in the adsorbent dosage. The adsorbed  $\text{PO}_4^{3-}$  increased from 12%, 56%, and 84% at 0.1  $\text{mg L}^{-1}$  adsorbent dosage to the maximum removal of 31%, 76% and 97.6% at 1.8  $\text{mg L}^{-1}$  adsorbent dosage for P, AFS and P-AFS respectively. It was attributed to the raise in the number of binding sites for the studied three materials [31]. Also, the accumulation of adsorbent particle and repulsive forces between binding sites may also improve the  $\text{PO}_4^{3-}$  removal [32]. The effect of the variation in  $\text{PO}_4^{3-}$  initial concentration affects to a little extent the adsorption efficiency.



**Figure 5.** Adsorption results of the materials to  $\text{PO}_4^{3-}$  anions. (A) Adsorption capacity of materials to  $\text{PO}_4^{3-}$  anions at different pH ranges. (B) Adsorption capacity of materials to  $\text{PO}_4^{3-}$  anions at different adsorbent dose. (C) Adsorption capacity of materials to  $\text{PO}_4^{3-}$  anions at different initial concentrations. (D) Adsorption capacity of materials to  $\text{PO}_4^{3-}$  anions at different time intervals.

#### Effect of time of $\text{PO}_4^{3-}$ adsorption

The time of reactions an important feature in the adsorption process. It describes the equilibrium point between  $\text{PO}_4^{3-}$  anions and sorbents, in addition tolerating  $\text{PO}_4^{3-}$  adsorption kinetics. The effect of time on  $\text{PO}_4^{3-}$  sorption was investigated by varying the reaction time from 5 to 180 min with an initial  $\text{PO}_4^{3-}$  concentration of  $27.72 \text{ mg L}^{-1}$  at  $\text{pH } 7 \pm 1.0$  and  $25 \text{ C}^0$ . It was observed that the initial concentration was decreased rapidly within the first 5 minutes of reaction time, and the  $\text{PO}_4\text{-P}$  concentration was decreased to  $0.8 \text{ mg/L}$  of  $\text{PO}_4\text{-P}$  following 3 hours. This means an average phosphate removal efficiency and adsorption capacity of 98.7 % and  $0.8 \text{ mg/L}$  of  $\text{PO}_4\text{-P}$  for the P-AFS composite.

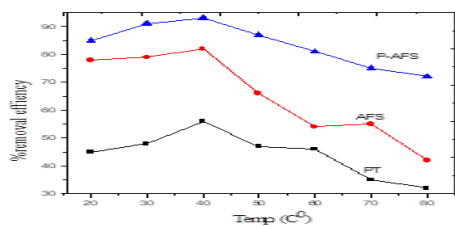


**Figure 6.** Adsorption capacity of materials to  $\text{PO}_4^{3-}$  anions at different temperatures ranges.

#### Temperature dependence of $\text{PO}_4^{3-}$ adsorption

The adsorption of phosphate anions onto the adsorbents was studied as a function of temperature at constant time Fig. (6). The effect of temperature is studied in the range of 0 to  $60 \text{ C}^0$ . It was obvious that the adsorption of  $\text{PO}_4^{3-}$  anions increased gradually with increase in temperature from 20 to  $60 \text{ C}^0$ , then reached its maximum at  $40 \text{ C}^0$  for PT, AFS, and P-AFS. The adsorption process is endothermic; and accessibility of more dynamic sites at a higher temperature may be one reason for the increase in adsorption.

**Modelling of adsorption kinetics:** two models were proposed to study the adsorption kinetic and dynamics of PT, AFS and P-AFS composites for  $\text{PO}_4^{3-}$  anions: the pseudo-first and the pseudo-second (PS) order models. The pseudo-second order equation derived from the adsorption equilibrium capacity assumes that the rate of activity of desorption sites is proportional to the square of the number of vacant sites [33]. The linearity of pseudo-second-order kinetic model [33] is expressed by equation (6).

$$\frac{t}{Q_e} = \frac{1}{K_2 Q_2} + \frac{1}{Q} t \quad (3)$$

Where  $k_2$  ( $\text{g mg}^{-1}\text{min}^{-1}$ ) is the rate constant of pseudo second-order reaction for adsorption, and  $q_e$  is the adsorption capacity calculated by the pseudo-second order model ( $\text{mg g}^{-1}$ ), and the pseudo-first order is given by the eq.

$$\ln(Q_e - Q_t) = \ln(Q_e) - \frac{k_1}{2.0303} t \quad (4)$$

Where  $k_1$  is the rate constant ( $\text{g mg}^{-1}\text{min}^{-1}$ ) of pseudo first-order kinetic model for adsorption and  $q_e$  is the adsorption capacity calculated by the pseudo-first order model ( $\text{mg g}^{-1}$ ).

Fig.(7, 8) show the appropriate closing of these two models and the complete parametric data are given in (table 1). It is obvious that the pseudo-first-order model ( $R^2=0.977, 0.88, 0.64$ ) for (P-AFS, AFS, PT, respectively), does not fit as well as the pseudo-second-order ( $R^2=0.998, 0.908, 0.901$ ) for (P-AFS, AFS, PT, respectively), the calculated  $q_e$  values from pseudo-second order model were in consistent with the experimental results ( $q_{\text{exp}}$ ). The well consistent of the pseudo-second-order model implies that the adsorption process is chemisorption. This conclusion was also recognized by the fitting of the Freundlich isotherm, and in accordance with the kinetic trends reported in the literature [34, 35].

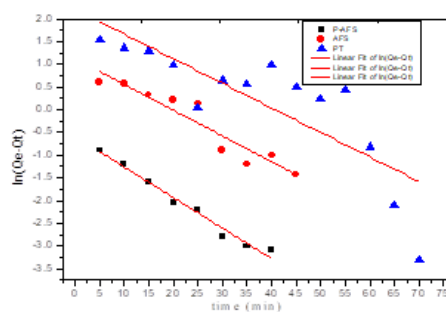


**Figure 7.** Pseudo-first-order-kinetic model of the  $\text{PO}_4^{3-}$  adsorption on PT, AFS, and P-AFS nanocomposite.

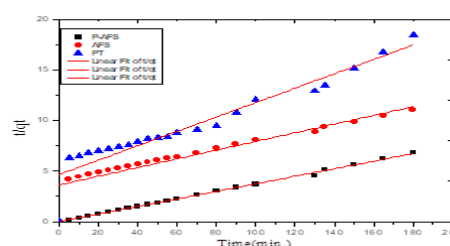


**Figure 8.** Pseudo-second-order-kinetic model of the  $\text{PO}_4^{3-}$  adsorption on PT, AFS, and P-AFS nanocomposite.

**Table 1.** Kinetic parameters of adsorption kinetic models of the  $\text{PO}_4^{3-}$  adsorption on PT, AFS, and P-AFS nanocomposite

Material	The pseudo first-order			The pseudo second order			
	$C_0(\text{mg l}^{-1})$	$q_{e(\text{exp})}(\text{mg/g})$	$q_e(\text{mg g}^{-1})$	$K_1(\text{min}^{-1})$	$R^2$	$q_e(\text{mg g}^{-1})$	$K_2(\text{min}^{-1})$
P-AFS 0.998	27.72	26.5	1.55	$1.3 \times 10^{-4}$	0.977	26.8	$8.7 \times 10^{-2}$
AFS 0.908	27.72	19.5	3.03	$1.1 \times 10^{-4}$	0.88	20.51	7.11
PT 0.902	27.72	12.8	9.02	$1.09 \times 10^{-4}$	0.64	14.12	1.08

**Modeling of adsorption isotherm:** in order to study the process of adsorption, the two models Langmuir and Freundlich were used to explicate the experimental data. The Langmuir model is suitable for adsorption of a particular monolayer of adsorbate with homogeneous surface. The form of the Langmuir isotherm can be expressed by the following equation.

$$q_e = q_m \frac{K_L C}{1 + K_L C} \quad (5)$$

Where  $q_m$  (the maximum capacity of adsorption,  $\text{mg/g}$ ) and  $K_L$  (a constant associated with the attraction of the binding sites,  $\text{L/mg}$ ) are the Langmuir isotherm constants. Both  $q_m$  and  $K_L$  can be determined from the linear Langmuir-II equation as:

$$\frac{C_e}{q_e} = \left( \frac{1}{K_L q_m} \right) + \frac{C_e}{q_m} \quad (6)$$

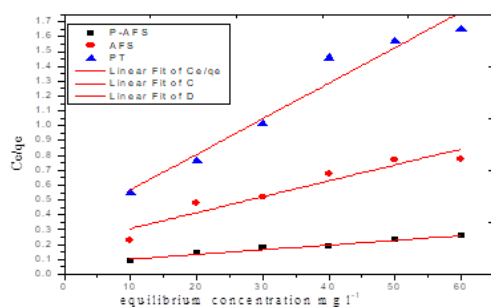
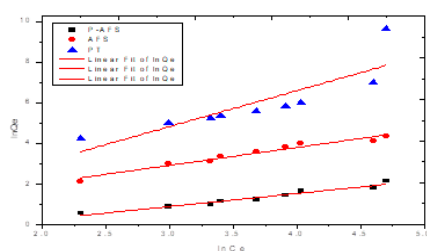
**Table 2. Langmuir and Freundlich isotherm parameters of of the  $\text{PO}_4^{3-}$  adsorption on PT, AFS, and P-AFS nanocomposite.**

Material	Langmuir			Freundlich		
	$q_m(\text{mg g}^{-1})$	$K_L$	$R^2_L$	$K_F(\text{mg g}^{-1})$	$1/n$	$R^2_F$
PT	43.4	0.070	0.645	1.609	1.76	0.693
AFS	100	0.050	0.892	1.332	1.02	0.957
P-AFS	344.8	0.040	0.96	0.352	0.64	0.996

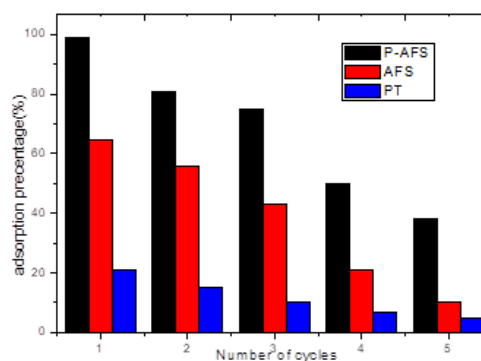
The Freundlich equation assumes that the adsorption process is a multilayer adsorption with heterogeneous surface. Both nonlinear and linear forms of Freundlich are given as:

$$\ln Q_e = \ln K_f + \frac{1}{n} \ln C_e \quad (7)$$

Where  $q_e$  is the quantity of ions adsorbed per gram of adsorbent ( $\text{mg g}^{-1}$ );  $C$  is the equilibrium ion concentration in solution;  $K_f$  and  $n$  are the Freundlich constants, which represent the adsorption capacity and the adsorption intensity, respectively. The magnitude of  $1/n$  indicates the adsorption isotherm is favourable or unfavourable and the degree of heterogeneity of the adsorbent surface. Applying the models of isotherm is more useful to understand the interaction between the adsorbent and  $\text{PO}_4^{3-}$ . So this information usually benefits to optimize, design and control the adsorption process, Fig. (9) and Fig.(10) show the isotherms based on the experimental data and the parameters obtained from linear regression analysis using adsorption models

**Figure 9.** Langmuir adsorption isotherm of  $\text{PO}_4^{3-}$  adsorption on PT, AFS, and P-AFS nanocomposite.**Figure 10.** Freundlich adsorption isotherm of  $\text{PO}_4^{3-}$  adsorption on PT, AFS, and P-AFS nanocomposite.

By comparing the regression coefficients ( $R^2$ ) of both models the Freundlich isotherm model provided a better fit with the adsorption data. The Freundlich constant,  $n$ , P-AFS composite was more than 1, favorable conditions for adsorption other than the two materials, which implies better efficiency.

**Figure 11.** Adsorption reusability of materials for  $\text{PO}_4^{3-}$  anions adsorption

## Conclusion

In summary, we have prepared and evaluated a composite material with adsorptive properties. The conjugated, covalently bonded material was insoluble in water. The P-AFS composite with nanoporous with 0.31 nm in diameter have been synthesized by a hard template method via a grafting of the silica precursors. Covalently bonded to pectin. The XRD showed that P-AFS composite is amorphous material. FT-IR spectra revealed chemical structure similar to the AFS material and PT, also the TEM and SEM analysis showed that this material is a nanosized porous material. The P-AFS composite material may offer a practical solution for the phosphate removal in terms of uptake capacity and recycle ability with highly efficiency comparable to reported pioneering  $\text{PO}_4^{3-}$ .

**Conflicts of interest**“ There are no conflicts to declare”

### Acknowledgments

I thank my colleagues for helpful discussions and assistance in STEM, XRD characterization. **funding:** the financial support of the present work by the National Research Centre and the Cairo University in Egypt is highly appreciated. **Author contributions:** SH. R., H.I., and M.S.SH. Supervised and coordinated all aspects of the project. M.H.G. synthesized and characterized the materials, carried out the measurements and the preliminary analysis.

### REFERENCES

1. Yokoi ,T., Syntheses and Applications of Well-ordered Porous Silica by using Anionic Surfactants and Basic Amino Acids, *Journal of the Japan Petroleum Institute*, **55**, (1), 13-26 (2012).
2. Wan ,Y., &Zhao ,D. Y., On the controllable soft-templating approach to mesoporous silicates. *Chem. Rev.* **107**, 2821–2860 (2007).
3. Schüth, F., &Schmidt ,W. , Microporous and mesoporous materials. *Adv. Mater.* **14**, 629–638 (2011).
4. Tanev , P.T., &Pinnavaia ,T.J., A neutral templating route to Mesoporous molecular sieves, *Science* **267**, 865e867, (2011)
5. Junkai,G.,Xiuwang, G., Wenwen,T.,Jinshu, L.D. C.,&Chen, Y. Norepinephrine-functionalised nanoflower-like organic silica as a new adsorbent for effective Pb(II) removal from aqueous solutions. *Scientific Reports*, **9**, 293, (2019).
6. Huang ,W. , Li ,D., Zhu ,Xu ,Y., ,Li ,K., Han ,J.,&Zhang, B., Y., Phosphate adsorption on aluminum-coordinated functionalized macroporous–mesoporous silica: Surface structure and adsorption behavior. *Materials Research Bulletin*, **48**, 4974– 4978, (2013).
7. Chouyyok,W., Wiacek, R.J. ,Pattamakomsan, K.,Sangvanich, T., Grudzien,R.M., Fryxell,G.E.&Yantasee,W., Phosphate removal by anion binding on functionalized nanoporous sorbents. *Environ. Sci. Technol.* **44**, 3073–3078, (2010) .
8. Zhang ,J., Shen ,Z.,Mei, Z., Li ,S.,&Wang ,W., removal of phosphate by Fe- coordinated amino functionalized 3D mesoporous silicates hybride materials, *J. Environ. Sci.* **23**, 199–205, (2011).
9. Garg, S., Soni,K., Kumaran ,G. M.,Bal, R., Marek ,K. G., Gupta ,J.K.,Sharma, L.D., &Dhar,G. M., Acidity and catalytic activities of sulfated zirconia inside SBA-15. *Catal. Today*, vol. **141**(1-2), 125-129 (2009).
10. Yuan , Z.Y., &Su ,B.L., Insights into hierarchically meso–macroporous structured mater. *J. Mater. Chem.* **16**, 663 – 677 (2006)
11. Chakravarty,S.Mohanty,A., &Sudha,T. N., Removal of Pb (II) ions from aqueous solution by adsorption using bael leaves (Aegle marmelos). *J. Hazard. Mater.* **173**, 502–509 (2010).
12. Repo ,E. , Warchoł,J. K. A. Bhatnagar,Mudhoo A., &Sillanpa,M. , Aminopolycarboxylic acid functionalized adsorbents for heavy metals removal from water, *water research*, **47** , 4812-4832(2013).
13. Hernandez,G. M., Lozano,N. C.,Renard, F.,&Quirico E., Removal of oxyanions from synthetic wastewater via carbonation process of calcium hydroxide: Applied and fundamental aspects, *Journal of Hazardous Materials* **166** , 788–795 (2009).
14. Daniel,J.,Conley, I. , Hans ,W., Robert ,W. P., Howarth,Donald ,W, Boesch,F., SeitzingerS. P. Havens , K. E.,Lancelot, C.,&LikensG. E., Controlling eutrophication: Nitrogen and Phosphorus, *Science* , **323**, 1014-1015, (2009).
15. A Technical Support Document prepared for Ohio Environmental Protection Agency by Tetra Tech. May, (2013)
16. Ruzhitskaya, O., &S.Gogina, E., Methods for Removing of Phosphates from Wastewater, MATEC Web of Conferences **106**, 07006 (2017).
17. Nigar,H.,Banos,B.G.,Felipe, L., Foix,P., &Civera,M. C., Amine-Functionalized Mesoporous Silica: A Material Capable of CO<sub>2</sub> Adsorption and Fast Regeneration by Microwave Heating, *AICHE Journal*, **62**, 547-555, (2016).
18. Yamada,M., &Shiiba,Sh., Preparation of pectin-inorganic composite material as Accumulative material of metal ions, *J. Appl. Polym. Sci.*, **132**, 1-7 (2015).
19. APHA (American Public Health Association), Standard methods for the examination of Water and Wastewater, (Washington, DC, USA APHA., 1995).
20. zucca, P.,&sanjust, E., Inorganic Materials as Supports for Covalent Enzyme Immobilization: Methods and Mechanisms, *Molecules*, **19**, 14139-14194 (2014).
21. Fajardo, A.R., Lopes ,L. C.,Pereira, A.G.B., RubiraA.F.,&Muni, E.C. Polyelectrolyte Complexes based on pectin–NH<sub>2</sub> and chondroitin sulfate, *Carbohydrate Polymers*, **87**,1950- 1955 (2012).

22. Sutar, P.B., Mishra, R.K., Pal ,K., Banthia, A.K., Development of pH sensitive Polyacrylamide Grafted pectin hydrogel for controlled drug delivery system, *Journal of Materials Science: Materials in Medicine*, **19**, 2247–2253(2008).
23. Kim, S., Ida, J., Guliants, V.V., Lin, J.Y.S. Tailoring pore properties of MCM-48 silica for selective adsorption of CO<sub>2</sub>, *J. Phys.*,**109** ,6287–6293 (2005).
24. Yokoi T.,Yoshitake, H., Yamada ,T., Kubota ,Y.,&Tatsumi, T., Design of functionalization and analysis of organically modified siliceous oxides with periodic structures for the development of sorbents for hazardous substances *J. Mater. Chem.* **16**, 1125–1135 (2006).
25. Yokoi,T. , Kubota,Y. ,&Tatsumi,T., Amino functionalized mesoporous silica as base catalyst and adsorbent, *Applied Catalysis A: General*, **421**, 14– 37(2012).
26. Horvat,G., Pantić,M., Knez,Ž., &Novak ,Z. , preparation and characterization of polysaccharide –silica hybrid aerogels,*Scientific Reports*, **9**, 16492, (2019).
27. Soderberg, T., Organic Chemistry with a Biological Emphasis volume II, *chemistry Publications.2.(University of Minnesota Morris*, 2019).
28. Nandi,B., Goswami, A., &Purkait,M., Adsorption characteristics of brilliant green dye on kaolin, *J. Hazard. Mater.* **161**, 387–395(2009).
29. Choi ,J., Chung ,J., Lee ,W.,&Kim, J. O., Phosphorous adsorption on synthesized magnetite in waste water, *J. Ind. Eng. Chem.***34** , 198–203(2016).
30. Ren ,Z., L., &Zhang ,S.G., Adsorption of phosphate from aqueous solution using an iron–zirconium binary oxide sorbent, *Water, Air, Soil Pollut.* **223**, 4221–4231(2012).
31. Yoon ,S.Y., Lee ,C.G., Park,J.A., Kim ,J.H., Kim ,S.B.,Lee, S.H., &Choi ,J.W., Kinetic, equilibrium and thermodynamic studies for phosphate adsorption to magnetic iron oxide nanoparticles, *Chem. Eng. J.* **236** , 341–347(2014).
32. MezennerN.Y.,&Bensmaili A., Kinetics and thermodynamic study of phosphate adsorption on iron hydroxide egg shell waste, *Chem. Eng. J.***147** , 87–96 (2009).
33. Chen ,Z., Ma ,W.,&Han M., Biosorption of nickel and copper onto treated alga (*Undaria pinnatifida*): Application of isotherm and kinetic models.*J. Hazard. Mater.***155**, 327–333(2008).
34. Mezenner,N.Y., &Bensmaili,A., Kinetics and thermodynamic study of phosphate adsorption on iron hydroxide-eggshell waste, *Chem. Eng. J.***147**, 87–96, (2009).
35. Rehman,M.S.U.,Munir, M., Ashfaq,M., Rashid ,N.,Nazar, M.F., Danish ,M., &Han,J.I. Adsorption of Brilliant Green dye from aqueous solution onto red clay, *Chem.Eng. J.* **228**, 54–62, (2013).